SUPPLEMENTARY MATERIALS

Strategies to improve CO tolerance and corrosion resistance of Pt electrocatalysts for polymer electrolyte membrane fuel cells: Sn-doping of the mixed oxide–carbon composite support

Irina Borbáth[1]*, Khirdakhanim Salmanzade[1], Zoltán Pászti[1], Andrei Kuncser[2], Dana Radu[2], Ștefan Neațu[2], Emília Tálas[1], István E. Sajó[3], Dániel Olasz[4], György Sáfrán[4], Ágnes Szegedi[1], Mihaela Florea[2], András Tompos[1]

[1]HUN-REN Research Centre for Natural Sciences, Institute of Materials and Environmental Chemistry, Magyar Tudósok körútja 2, H-1117 Budapest, Hungary
[2]National Institute of Materials Physics, 405A Atomistilor Street, 077125, Magurele, Romania
[3]University of Pécs, Szentágothai Research Centre, Ifjúság u. 20. H-7624, Pécs, Hungary
[4]HUN-REN Centre for Energy Research, Institute for Technical Physics and Materials Science, Konkoly-Thege Miklós út 29-33, H-1121, Budapest, Hungary

* Corresponding author, Tel.: +36 1 382 6916, email: borbath.irina@ttk.hu, address: H-1519 Budapest, P.O.Box 286, Hungary (Irina Borbáth)

1. Experimental

1.1 Synthesis of the 25 wt.% $Ti_{0.8}Sn_{0.2}O_2$ - 75 wt.% C composites - Route B

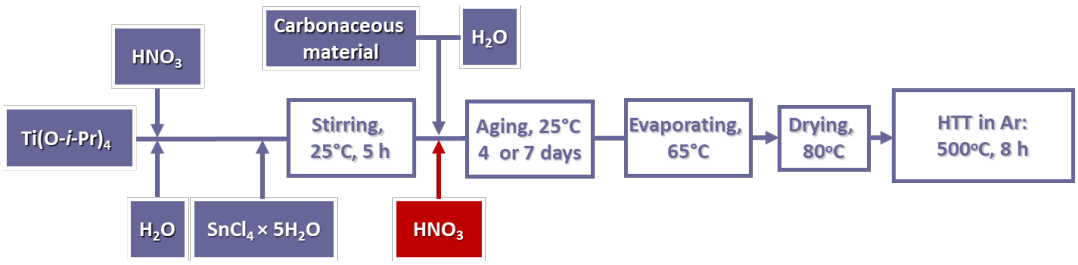

Figure S1. Preparation steps of 25 wt.% $Ti_{0.8}Sn_{0.2}O_2$- 75 wt.% C composites via route ***B*** (HTT: high-temperature treatment).

Our results with the Mo-doped systems demonstrate [1] that when preparing composite materials with the $Ti_{0.8}Mo_{0.2}O_2$/C= 25/75 ratio, aging the synthesis mixture at room temperature for 4 days is not always sufficient to prepare a pure TiO_2-rutile phase. The difference between the preparations of two 25Sn02 and 25Sn02-7 samples with high carbon content was the duration of the aging step, which was 4 and 7 days, respectively (see Figure S1).

2. Results

2.1 Results of physicochemical characterization

Raman spectroscopy measurements

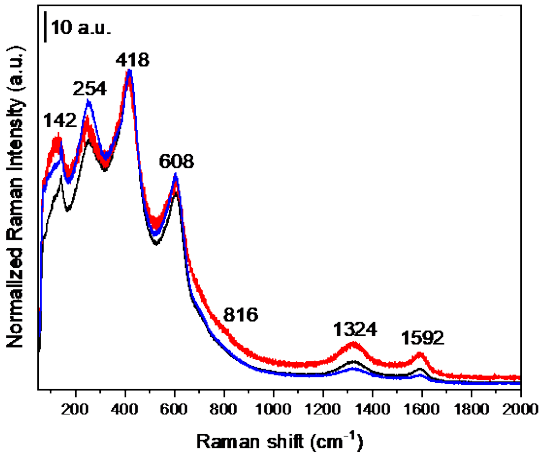

Figure S2. Raman spectra of the $Ti_{(1-x)}Sn_xO_2$–C (x: 0.1, 0.2 and 0.3) composite materials prepared by route ***A***: 75Sn01/A (■), 75Sn02/A (■) and 75Sn03/A (■).

Figure S2 shows the Raman spectra of the $Ti_{(1-x)}Sn_xO_2$–C (x: 0.1, 0.2 and 0.3) composite materials containing 75 wt.% of mixed oxides and 25 wt.% Black Pearls 2000 carbon. These composites prepared by route ***A*** present distinct Raman signatures for both Ti–O–Ti and C–C/C=C bonds. Thus, all spectra show the typical TiO_2 rutile type Raman-active optical phonon modes centered at 142, 418 and 608 cm^{-1} attributed to the B_{1g}, E_g and A_{1g} modes, respectively. The band located at 254 cm^{-1}, fully developed also in all our Raman spectra, represents a combined line typically appearing when the degree of distortion is high [2,3]. The weak high-frequency line of the B_{2g} symmetry, centered at 816 cm^{-1}, are poorly observed in our measurements. The Raman spectra of these materials do not contain lines corresponding to SnO_2.

On the other hand, the presence of graphitic carbon in the composites has been demonstrated clearly by the corresponding D and G bands for the carbon materials, all spectra showing the first-order Raman lines at 1324 and 1592 cm^{-1} [4,5]. The D band corresponds to the disordered graphitic lattices usually assigned to K-point phonons of A_{1g} symmetry, while the G band is a signature of an ideal graphitic lattice, this former band being assigned to the Raman-active E_{2g} mode for the tangential in-plane stretching vibrations of the sp^2-hybridized bond [6,7].

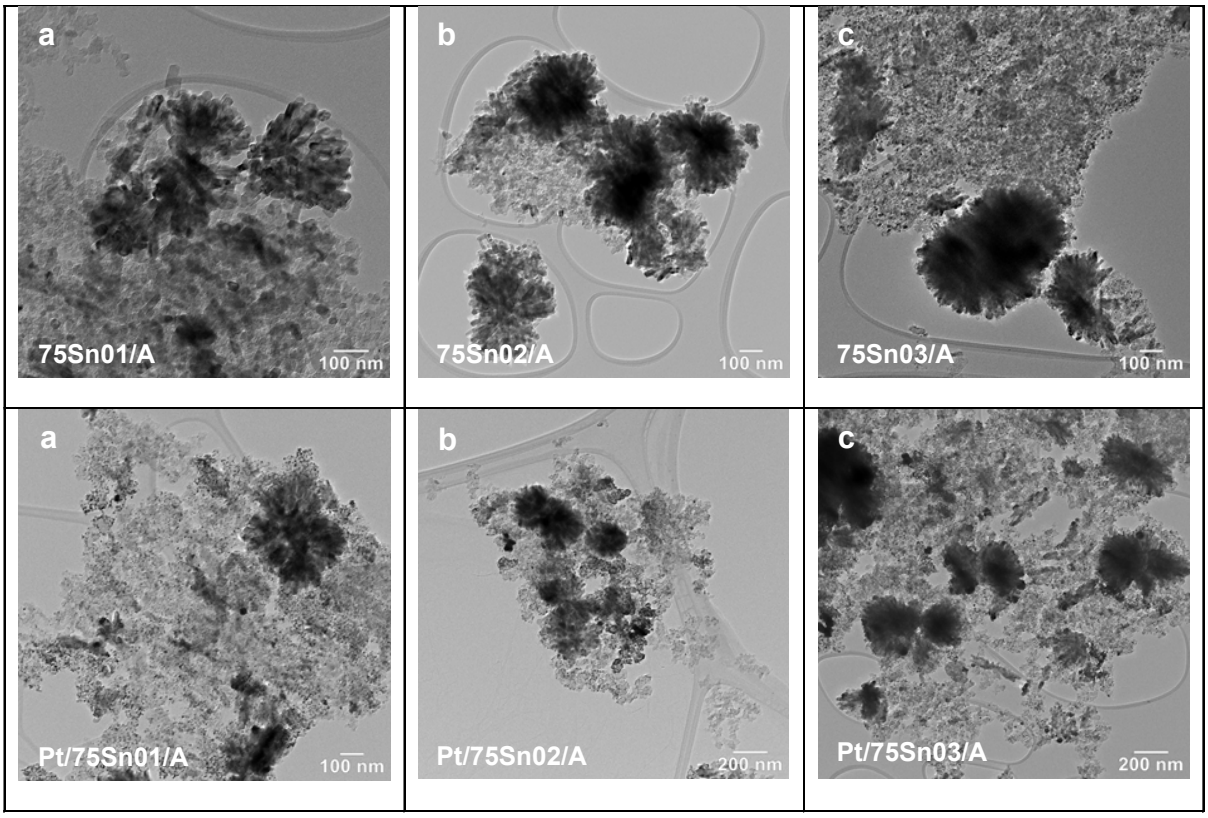

Figure S3. TEM overview micrographs of the 75 wt.% $Ti_{(1-x)}Sn_xO_2$–25 wt.% C composite materials prepared by route ***A*** (top) and related Pt catalysts (bottom): x= 0.1 (a), x= 0.2 (b) and x= 0.3 (c).

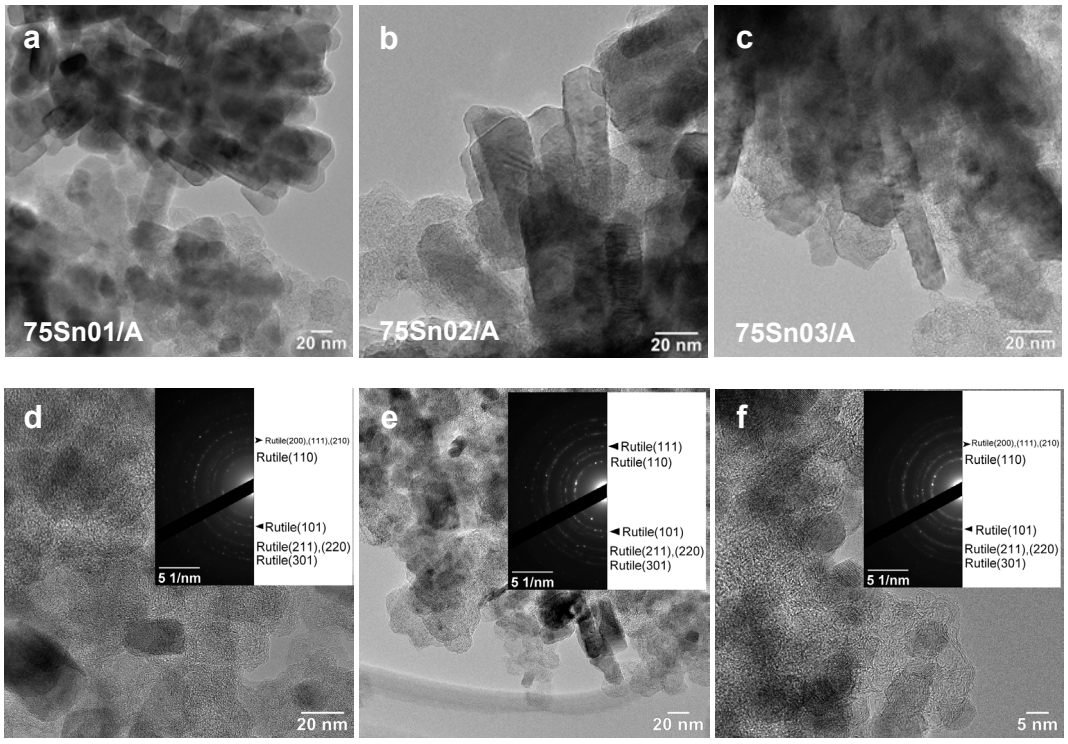

Figure S4. TEM micrographs and electron diffraction patterns of the 75 wt.% $Ti_{(1-x)}Sn_xO_2$–25 wt.% C composite materials prepared by route ***A***: x= 0.1 (a, d), x= 0.2 (b, e) and x= 0.3 (c, f).

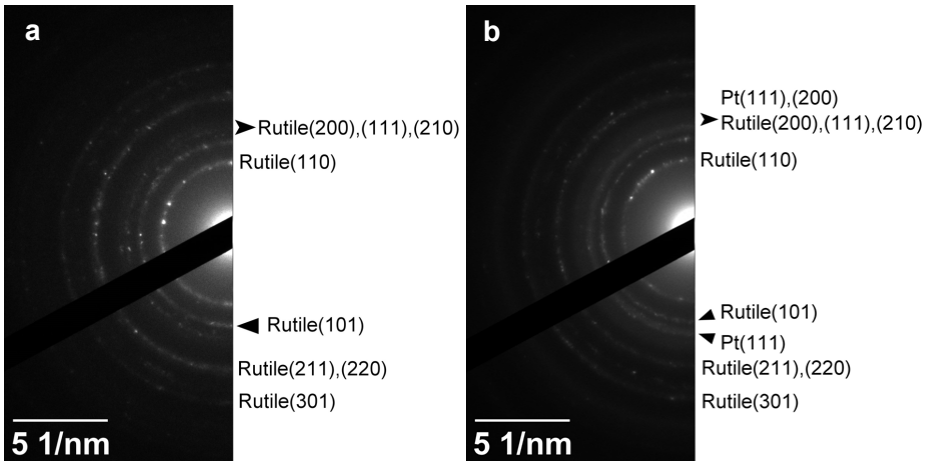

Figure S5. Comparison of the electron diffraction pattern of 75SnO3/A composite support material with Ti/Sn= 70/30 (a) and Pt/75SnO3/A catalyst (b). After Pt loading a somewhat broad ring overlapping with the faint rutile (200), (111) or (210) rings confirmed the presence of nanosized metallic Pt particles in the electrocatalyst.

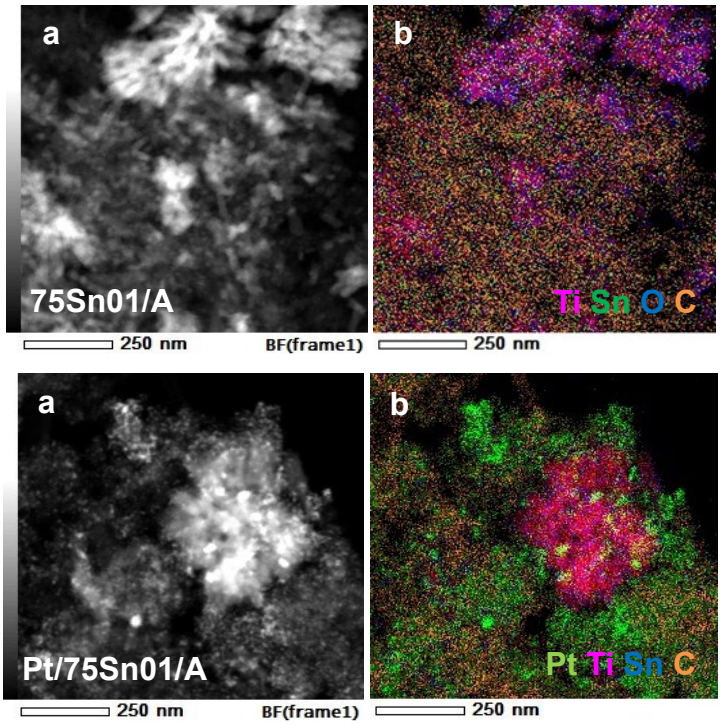

Figure S6. HAADF images (a) of the selected fragment of composite support material with Ti/Sn= 90/10 (top) and related Pt/75Sn01/A catalyst (bottom) and EDS elemental maps of all elements obtained over this area (b).

HAADF images of the selected fragment and overview EDS elemental maps of all elements obtained over this area of composite support material with Ti/Sn= 90/10 and related Pt/75Sn01/A catalyst are compared on Figure S6. In particular, Ti/Sn ratios measured by STEM-EDS on the nanorod-like crystallites or their flower-like agglomerates coincided very well with the nominal composition data (Ti/Sn ~ 9:1 and Ti/O ~ 1:2). However, it is not excluded that in composites prepared by route ***A*** certain amount of tin is also distributed over the carbon. The elemental

distribution pattern of Pt shown in Figure S6 (bottom) confirmed that Pt settled on both the large mixed oxide features and on the more homogeneous parts of the composite support.

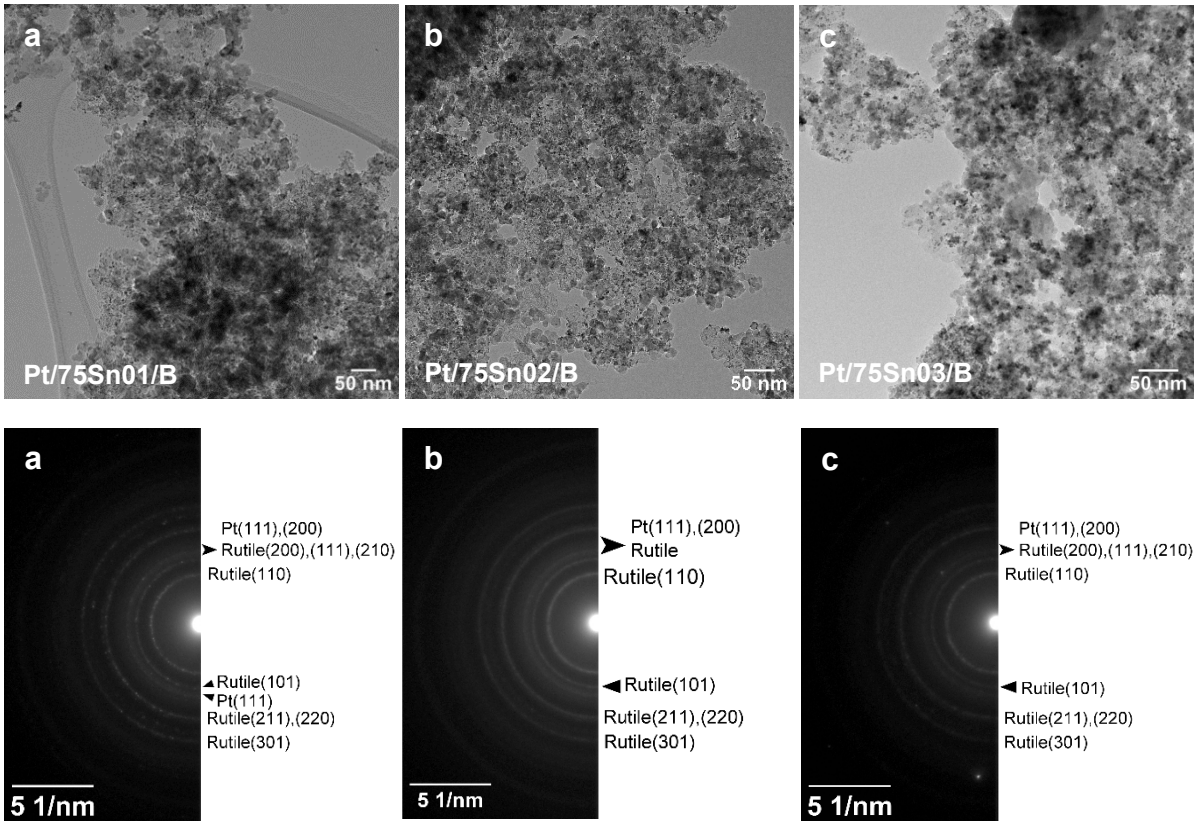

Figure S7. TEM micrographs and electron diffraction patterns of the Pt catalysts on 75 wt.% $Ti_{(1-x)}Sn_xO_2$–25 wt.% C composite materials prepared by route ***B***: x= 0.1 (a), x= 0.2 (b) and x= 0.3 (c).

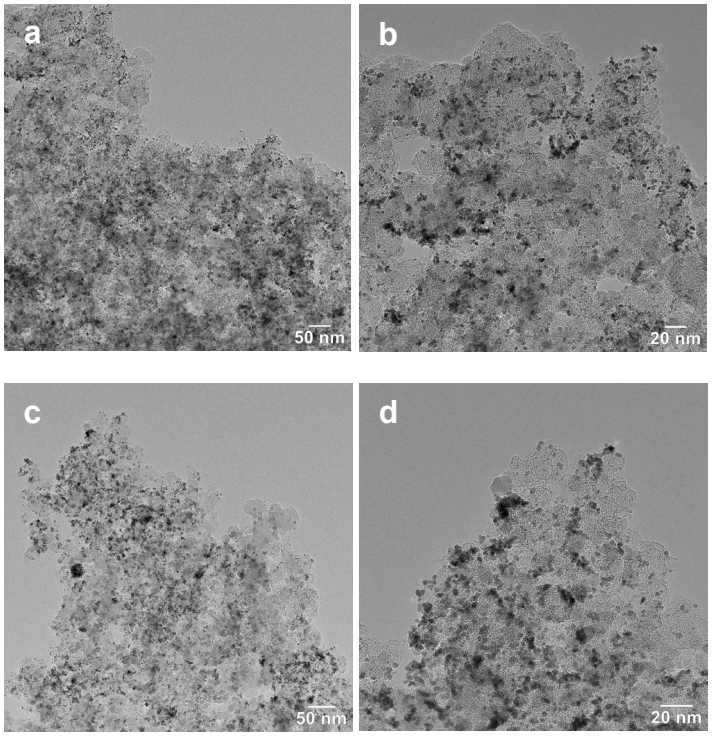

Figure S8. TEM images of the Pt/25Sn02 electrocatalysts: Pt/25Sn02/B (a, b) and Pt/25Sn02/B-7 sample with prolonged aging step (c, d).

Energy dispersive X-ray (EDX) spectroscopy measurements

Table S1. Characterization of selected areas of $Ti_{(1-x)}Sn_xO_2$–C composite supported Pt catalysts by EDX; the nominal composition is given for comparison.

Sample ID	Ti/Sn (at/at)		$TiSnO_x$/C (wt.%/wt.%)		Pt [a] (wt.%)
	Nominal	EDX	Nominal	EDX	
Route A					
75Sn01/A	90/10	92/8	75/25	66/34	-
75Sn02/A	80/20	85/15	75/25	59/41	-
75Sn03/A	70/30	75/25	75/25	77/23	-
Pt/75Sn01/A	90/10	92/8	75/25	82/18	22.1
Pt/75Sn02/A	80/20	84/16	75/25	84/16	18.6
Pt/75Sn03/A	70/30	77/23	75/25	62/38 [b]	10.6 [b]
Route B					
Pt/75Sn01/B	90/10	91/9	75/25	89/11	17.3
Pt/75Sn02/B	80/20	84/16	75/25	91/9	21.0
Pt/75Sn03/B	70/30	78/22	75/25	89/11	22.2
Pt/25Sn02/B	80/20	83/17	25/75	46/54	18.4
Pt/25Sn02/B-7	80/20	83/17	25/75	46/54	20.6

[a] The nominal Pt content: 20 wt.%;
[b] Taken from sample region poor in Pt; the content of Pt is verified by ICP-OES measurements and is 19.1 wt.%.

SEM/EDX technique was used for the investigation of the morphology of composite supported Pt electrocatalysts; selected results obtained on the $Pt/Ti_{0.8}Sn_{0.2}O_2$–C electrocatalysts with high and low carbon content prepared using composite synthesized via route ***B*** are shown in Figure S9. Table S1 contains the results of the characterization by EDX of selected areas of $Ti_{(1-x)}Sn_xO_2$–C composite supported Pt catalysts (results obtained on composites prepared by route ***A*** are also included). The reason that EDX characterization of the composites synthesized via route ***A*** was carried out is the significant inhomogeneity of these materials demonstrated by TEM. Ti/Sn ratios of composite materials calculated from the results of EDX measurements were quite close to the nominal values. This result is not surprising since the method we used to prepare $Ti_{(1-x)}Sn_xO_2$–C supports does not involve steps where loss of tin or titanium would be expected (see Figure 1). Based on the minimal difference between the results presented in Table S1 and the nominal Ti/Sn values calculated for the Pt electrocatalysts, it can be concluded that, in contrast to catalysts containing Mo, the problem associated with the possibility of partial dissolution of the less stable (not incorporated into the TiO_2 lattice) Mo species during the deposition of Pt, mentioned in ref. [8], is not observed in the synthesis of tin-containing Pt electrocatalysts. Thus, the deposition of Pt does not lead to a change in the Ti/Sn atomic ratios of Sn-containing composite support materials.

Previously we demonstrated [9] that the Pt content obtained from the EDX data is highly dependent on the areas selected for analysis: the content of Pt measured by the EDX in the regions of the catalyst enriched in mixed oxide is in good agreement with the nominal value. Based on this, it can be assumed that Pt nanoparticles have a high affinity to concentrate on the mixed oxide.

Thus, EDX studies of all $Pt/Ti_{(1-x)}Sn_xO_2$–C (x: 0.1, 0.2 and 0.3) electrocatalysts have mainly focused on regions rich in mixed oxides, so the carbon content data is significantly lower than nominal. Thus, the $TiSnO_x$/C weight ratio indicated somewhat more oxide in the analyzed area than the nominal value. Nevertheless, as noted above, this deviation may be connected to the selection of the analyzed area. In this regard, a good example can be the results obtained on the Pt/75Sn03/A catalyst (see Table S1): in the selected area, the carbon content was higher, but the Pt content was significantly lower than nominal. However, the content of Pt in this sample was verified by ICP-OES measurements (Pt: 19.1 wt.%) and showed good agreement with nominal value.

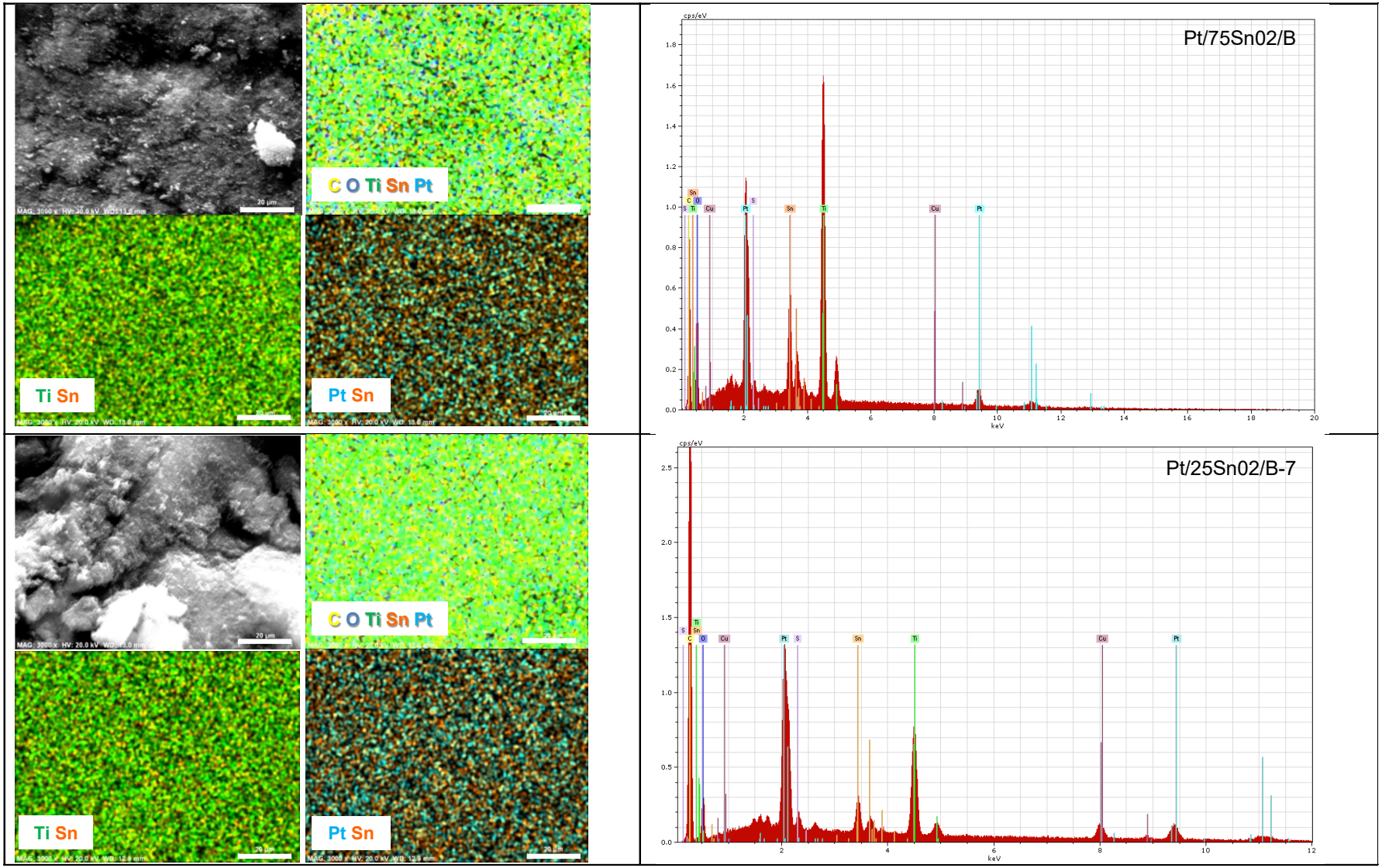

Figure S9. SEM images and EDX elemental analysis of the Pt/75Sn02/B (at the top) and the Pt/25Sn02/B-7 catalysts (at the bottom); scale bar: 20 µm

XPS measurements

Table S2. Surface composition data obtained by XPS on **75Sn02/A** and **75Sn02/B** composites during simulated HTT in 300 mbar Ar in the electron spectrometer

Sample ID & Treatment	**$TiSnO_x$/C (wt.%/wt.%)**	**Ti/Sn (at/at)**	**Sn^0 a)**	**$Ti_{1-x}Sn_xO_2$**
75Sn02/A				
without HTT	66/34	0.41:1	-	$Ti_{0.29}Sn_{0.71}O_2$
300 °C, 8 h	57/43	0.67:1	-	$Ti_{0.40}Sn_{0.60}O_2$
400 °C, 8 h	56/44	0.86:1	1-2%	$Ti_{0.46}Sn_{0.54}O_2$
500 °C, 8 h	55/45	1.00:1	3-12% b)	$Ti_{0.50}Sn_{0.50}O_2$
600 °C, 8 h	52/48	1.17:1	3-15% b)	$Ti_{0.54}Sn_{0.46}O_2$
75Sn02/B				
500 °C, 8 h	73/27	1.62:1	-	$Ti_{0.62}Sn_{0.38}O_2$
600 °C, 8 h	72/28	1.45:1	<2%	$Ti_{0.59}Sn_{0.41}O_2$
700 °C, 8 h	66/34	1.53:1	25%	$Ti_{0.60}Sn_{0.40}O_2$

a) Sn^0 fraction with respect to the total tin content; values of 2-3% are at the detection limit;
b) Strong spatial fluctuation in the amount of the metallic tin fraction, so its distribution in the sample was quite inhomogeneous.

The significant change of the oxide/carbon ratio in **75Sn02/A** around 300 °C suggests that sintering of the oxide occurs already in the initial phases of HTT, while improvement of the tin incorporation requires much higher temperatures.

Data presented in Table S2 indicate only a slight structural change in the **75Sn02/A** and **75Sn02/B** composites during HTT between 500 and 600 °C, therefore we consider it acceptable to compare **75Sn02/A** treated at 600 °C (to adhere to the conditions of traditional synthesis) and **75Sn02/B** treated at 500 °C. Based on the presented results, we believe that the differences in the microstructure (e.g., in TiO_2 dispersion or segregated nature of Sn) are already present at the end of the sol-gel process.

2.2. Results of electrochemical characterization

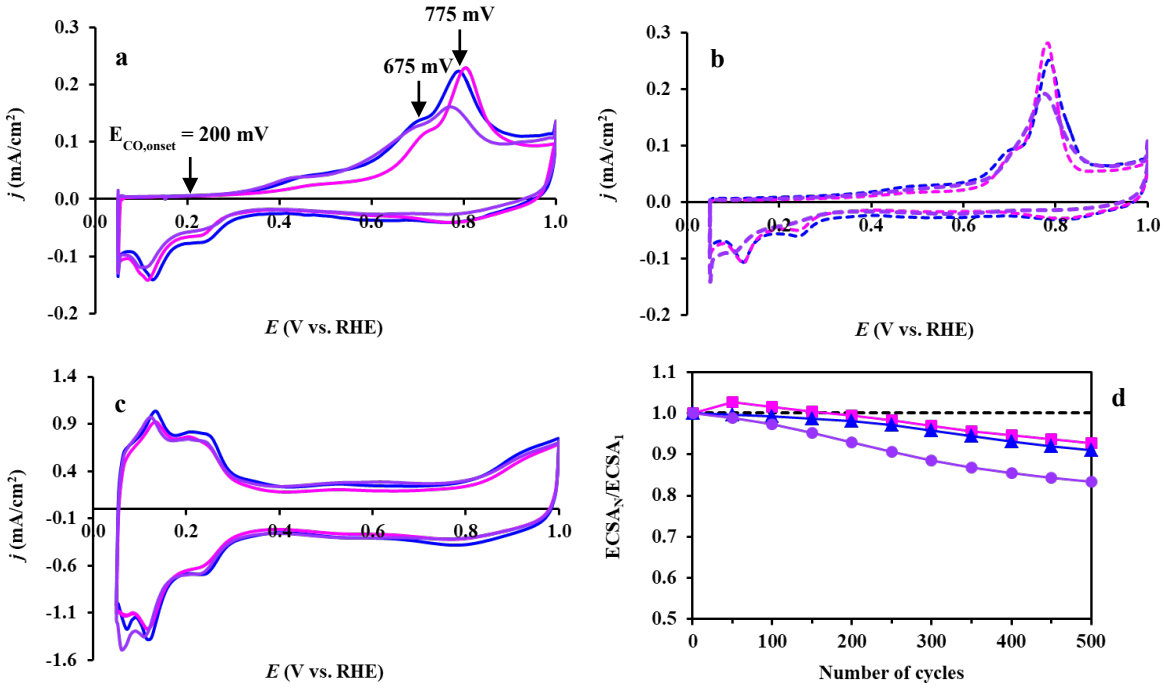

Figure S10. Effect of the Ti/Sn ratios in $Ti_{(1-x)}Sn_xO_2$–C composite materials on the electrochemical performance of the catalysts prepared by route ***B***. CO_{ads} stripping voltammograms of the electrocatalysts obtained before (a) and after the 500-cycle stability test (b); CVs of the fresh electrocatalysts (c), and ECSA change during 500 CV cycles (d): comparison of the ECSA measured after N cycles normalized to ECSA measured in the 1st cycle ($ECSA_N/ECSA_1$) of the Pt/75Sn01/B (■), Pt/75Sn02/B (■) and Pt/75Sn03/B (■) catalysts as a function of the number of cycles (N). Recorded in 0.5 M H_2SO_4 at 10 mV s^{-1} (a, b) and 100 mV s^{-1} (c), T= 25 °C.

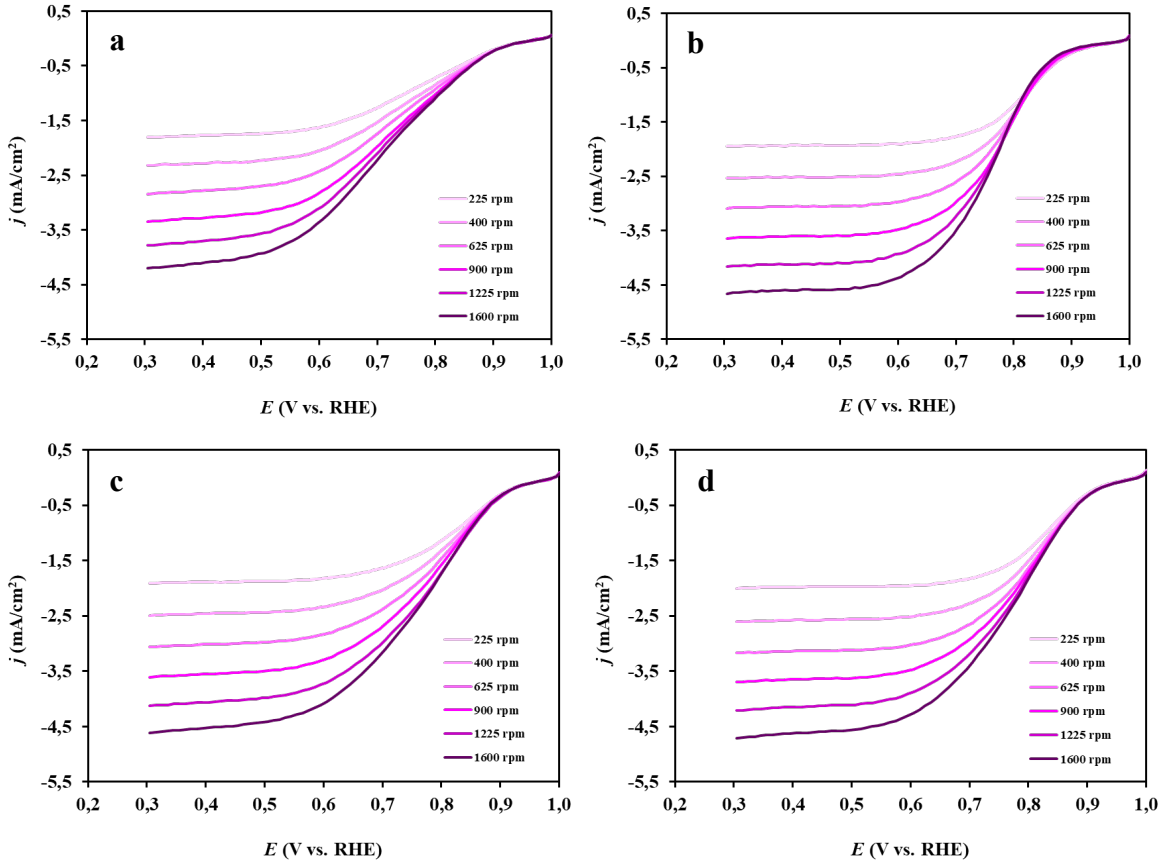

Figure S11. Potentiodynamic (10 mV s^{-1}, negative sweep) oxygen reduction current densities obtained in O_2-saturated 0.5 M H_2SO_4 at 225, 400, 625, 900, 1225 and 1600 rpm: (a) Pt/75Sn02/B, (b) Pt/25Sn02/B, (c) Pt/25Sn02/B-7, and (d) reference Pt/C electrocatalyst (20 wt.% Pt/C, Quintech). Current values were normalized to the geometric surface area of the GC electrode; the Pt loading of the electrodes was 10 µg cm^{-2}.

Potentiodynamic (10 mV s^{-1}, negative sweep) oxygen reduction current densities obtained in O_2-saturated 0.5 M H_2SO_4 at six rotation rates on the catalysts presented in Figure 10 were compared on Figure S11. The expected current density increase in the potential dynamic polarization curves at higher rotation rates (see Figure S11) was demonstrated for all catalysts, indicating faster diffusion of oxygen to the surface of catalysts.

In the presence of an intact, non-porous catalyst layer, the diffusion-limited current density (j_{lim}) on the working electrode should theoretically always be the same, since it depends solely on the rotation speed according to the Koutecký–Levich equation. However, according to the literature, the lower j_{lim} can be attributed to reversible oxide formation/reduction on Pt [10] or to the different morphology and/or structural characteristics of the support. Moreover, it should be noted that the deviation of j_{lim} values observed in Figure 10 was within the range of expected relative measurement errors mentioned by Mayrhofer *et al.* [11] for j_{lim} values observed in the ORR measurements on carbon-containing supported catalysts, which were about 10%.

We adhere to the widespread opinion in the literature that the interpretation of the results of RDE measurements on electrocatalysts with large surface area and disperse surface have to carried out cautiously [12,13]. Nevertheless, in our case catalyst samples with similar composition and structure were investigated applying the same procedure and electrode preparation technique and the RDE results may contribute to the qualitative description and comparison the catalysts. Moreover, activity of the catalysts was compared with the results obtained on the commercial reference Pt/C (20 wt.% Pt/C, Quintech).

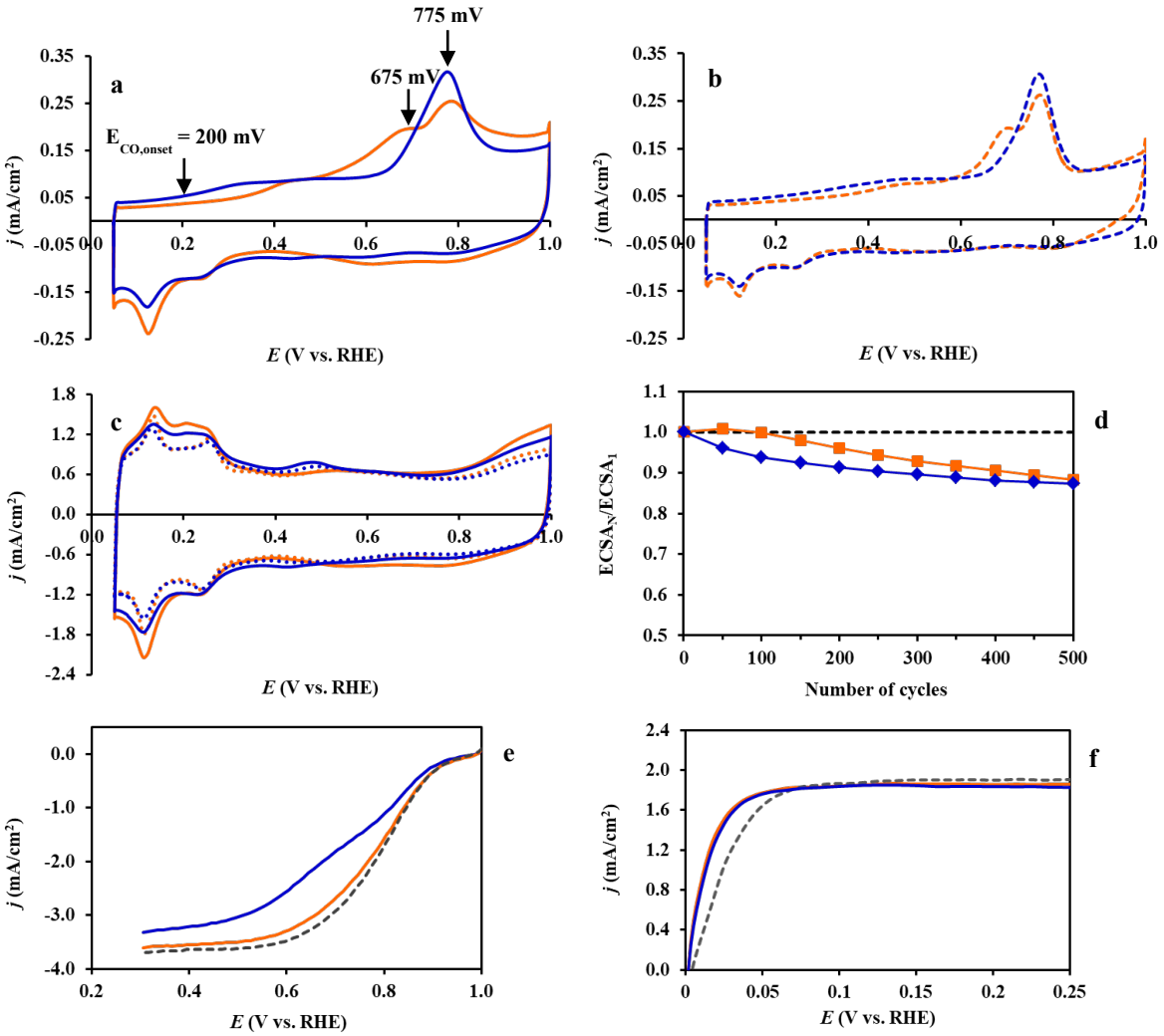

Figure S12. Effect of the type of doping metal on the electrochemical performance of the 20 wt.% Pt/25 wt.% $Ti_{0.8}M_{0.2}O_2$-75 wt.% C (M: Mo (■), Sn (■)) electrocatalysts. CO_{ads} stripping voltammograms obtained before (a) and after the 500-cycle stability test (b), CVs recorded before and after 500 cycles (c), ECSA change during 500 CV cycles (d), results of the RDE measurements at 900 rpm in the ORR (e) and the HOR (f) (the reference Pt/C (■) was included for comparison). The CVs were recorded in 0.5 M H_2SO_4 before (solid curves) and after 500 cycles (dotted curves) of the stability test. Sweep rate: (a, b, e, f) 10 mV s^{-1} and (c) 100 mV s^{-1}, T= 25 °C.

References

[1] I. Borbáth, K. Zelenka, Á. Vass, Z. Pászti, G.P. Szijjártó, Z. Sebestyén, G. Sáfrán, A. Tompos, CO tolerant Pt electrocatalysts for PEM fuel cells with enhanced stability against electrocorrosion, Int. J. Hydrogen Energy. 46 (2021) 13534–13547. https://doi.org/10.1016/j.ijhydene.2020.08.002.

[2] S.P.S. Porto, P.A. Fleury, T.C. Damen, Raman spectra of TiO_2, MgF_2, ZnF_2, FeF_2, and MnF_2, Phys. Rev. 154 (1967) 522–526. https://doi.org/10.1103/PhysRev.154.522.

[3] M. Gotić, M. Ivanda, S. Popović, S. Musić, A. Sekulić, A. Turkovic, K. Furić, Raman investigation of nanosized TiO_2, J. Raman Spectrosc. 28 (1997) 555–558. https://doi.org/10.1002/(sici)1097-4555(199707)28:7<555::aid-jrs118>3.3.co;2-j.

[4] A.C. Ferrari, J. Robertson, Interpretation of Raman spectra of disordered and smorphous carbon, Phys. Rev. B. 61 (2000) 14095. https://doi.org/10.1007/BF02543692.

[5] K.N. Kudin, B. Ozbas, H.C. Schniepp, R.K. Prud'homme, I.A. Aksay, R. Car, Raman spectra of graphite oxide and functionalized graphene sheets, Nano Lett. 8 (2008) 36–41. https://doi.org/10.1021/nl071822y.

[6] Z. Tian, C. Liu, Q. Li, J. Hou, Y. Li, S. Ai, Nitrogen- and oxygen-functionalized carbon nanotubes supported Pt-based catalyst for the selective hydrogenation of cinnamaldehyde, Appl. Catal. A Gen. 506 (2015) 134–142. https://doi.org/10.1016/j.apcata.2015.08.023.

[7] F. Tuinstra, J.L. Koenig, Raman Spectrum of Graphite, J. Chem. Phys. 53 (1970) 1126–1130. https://doi.org/10.1063/1.1674108.

[8] Á. Vass, I. Borbáth, Z. Pászti, I. Bakos, I.E. Sajó, P. Németh, A. Tompos, Effect of Mo incorporation on the electrocatalytic performance of Ti–Mo mixed oxide–carbon composite supported Pt electrocatalysts, React. Kinet. Mech. Catal. 121 (2017) 141–160. https://doi.org/10.1007/s11144-017-1155-5.

[9] I. Ayyubov, E. Tálas, K. Salmanzade, A. Kuncser, Z. Pászti, Ș. Neațu, A.G. Mirea, M. Florea, A. Tompos, I. Borbáth, Electrocatalytic Properties of Mixed-Oxide-Containing Composite-Supported Platinum for Polymer Electrolyte Membrane (PEM) Fuel Cells, Materials (Basel) 15 (2022) 3671. https://doi.org/10.3390/ma15103671.

[10] G. Alkan, V.P. M. Košević, M. Mihailović, S. Stopic, B. Friedrich, J. Stevanović, V. Panić, Characterization of Defined Pt Particles Prepared by Ultrasonic Spray Pyrolysis for One-Step Synthesis of Supported ORR Composite Catalysts. Metals (Basel) 12 (2022) 290. doi:10.3390/met12020290.

[11] K.J.J. Mayrhofer, D. Strmcnik, B.B. Blizanac, V. Stamenkovic, M. Arenz, N.M. Markovic, Measurement of oxygen reduction activities via the rotating disc electrode method: From Pt model surfaces to carbon-supported high surface area catalysts, Electrochim. Acta 53 (2008) 3181–3188. https://doi.org/10.1016/j.electacta.2007.11.057.

[12] J. Masa, C. Batchelor-McAuley, W. Schuhmann, R.G. Compton, Koutecky-Levich Analysis Applied to Nanoparticle Modified Rotating Disk Electrodes: Electrocatalysis or Misinterpretation. Nano Res. 7 (2014) 71–78. doi:10.1007/s12274-013-0372-0.

[13] C. Batchelor-McAuley, R.G. Compton, Thin-Film Modified Rotating Disk Electrodes: Models of Electron-Transfer Kinetics for Passive and Electroactive Films. J. Phys. Chem. C 118 (2014) 30034–30038. doi:10.1021/jp5104593.